Atmos. Chem. Phys. Discuss., https://doi.org/10.5194/acp-2018-1361
Manuscript under review for journal Atmos. Chem. Phys.
Discussion started: 7 February 2019

Atmospheric Chemistry and Physics Discussions

Winter 2018 major sudden stratospheric warming impact on midlatitude mesosphere from microwave radiometer measurements

Yuke Wang[1], Valery Shulga[1,2], Gennadi Milinevsky[1,3], Aleksey Patoka[2], Oleksandr Evtushevsky[3], Andrew Klekociuk[4,5], Wei Han[1], Asen Grytsai[3], Dmitry Shulga[2], Valery Myshenko[2], Oleksandr Antyufeyev[2]

[1]College of Physics, International Center of Future Science, Jilin University, Changchun, 130012, China
[2]Institute of Radio Astronomy, NAS of Ukraine, Kharkiv, 61002, Ukraine
[3]Taras Shevchenko National University of Kyiv, Kyiv, 01601, Ukraine
[4]Antarctica and the Global System, Australian Antarctic Division, Kingston, 7050, Australia
[5]Antarctic Climate and Ecosystems Cooperative Research Centre, Hobart, 7000, Australia

Correspondence to:
Gennadi Milinevsky (genmilinevsky@gmail.com) and Valerii Shulga (shulga@rian.kharkov.ua)

Abstract. The impact of a major sudden stratospheric warming (SSW) in the Arctic in February 2018 on the mid-latitude mesosphere was investigated by performing microwave radiometer measurements of carbon monoxide (CO) and zonal wind above Kharkiv, Ukraine (50.0°N, 36.3°E). The mesospheric peculiarities of this SSW event were observed using recently designed and installed microwave radiometer in East Europe for the first time. The data from the ERA-Interim and NCEP–NCAR reanalyzes, as well as the Aura Microwave Limb Sounder measurements, have been also used. Microwave observations of the daily CO profiles in January–March 2018 allowed retrieving mesospheric zonal wind at 70–85 km (below the winter mesopause) over the Kharkiv site. The reverse of the mesospheric westerly from about 10 ms^{-1} to the easterly wind of about –10 ms^{-1} around 10 February has been registered. Local microwave observations in the NH midlatitudes combined with reanalysis data show wide ranges of daily variability in CO, zonal wind, temperature and geopotential height in the mesosphere and stratosphere during the SSW 2018. Oscillations in the vertical CO profile, zonal wind, and geopotential height during the SSW, stratopause disappearance after the SSW onset and strong CO and westerly wind peaks at the start of the SSW recovery phase have been observed. The observed CO variability can be explained by vertical and horizontal air mass redistribution due to planetary wave activity with the replacement of the CO-rich air by CO-poor air and vice versa, in agreement with other studies. The results of microwave measurements of CO and zonal wind in the midlatitude mesosphere at 70–85 km altitudes, which still is not adequately covered

by ground-based observations, are useful for improving our understanding of the SSW impacts in this region.

1 Introduction

The event of major sudden stratospheric warming (SSW) which happened roughly each two years in the North Polar region is produced by strong planetary wave activity according to the model developed by Matsuno (1971) and numerous observations (Alexander and Shepherd, 2010; Kuttippurath and Nikulin, 2012; Tao et al., 2015). The major SSW event is accompanied by sharp increase of the stratosphere temperature up to 50 K and zonal wind reverse from climatologically eastward to westward during several days (Chandran and Collins, 2014; Butler et al., 2017). The World Meteorological Organization primary definition of the SSW event concentrated on stratosphere temperature increase and zonal wind reverse to westward at about 30 km altitude (10-hPa pressure level) and 60° latitude (WMO, 1978). This definition was broadened and detailed in recent papers (Butler et al., 2015; Butler and Gerber, 2018). The summarizing paper, where the SSW database described, was published in (Butler et al., 2017). This useful tool (https://www.esrl.noaa.gov/csd/groups/csd8/sswcompendium/) allows analysis of the conditions in the stratosphere, troposphere, and at the surface before, during and after each SSW event representing its evolution, structure and impact on winter surface climate.

The source of the SSW is planetary waves born in the troposphere that propagate upward through the tropopause to the stratosphere (Matsuno, 1971; Alexander and Shepherd, 2010, Butler et al., 2015). Due to the enhanced planetary wave activity, sharp increase in upward transfer of the momentum and heat, as estimated by Eliassen-Palm (EP) flux, results in rapid warming of the polar stratosphere and stratospheric polar vortex breakdown (Matsuno, 1971; de la Torre et al., 2012; Chandran and Collins, 2014; Pedatella et al., 2018). The important feature of the SSW event is impact on lower altitudes, when temperature and wind anomalies descend downward into the high- and mid-latitude troposphere during the weeks or even month and influence the surface weather (Baldwin and Dunkerton, 2001; Zhou et al., 2001; Butler et al., 2015; Yu et al., 2018). The major SSW events may also impact the atmosphere composition of the whole Northern Hemisphere (NH) stratosphere including mid-latitudes (Solomon et al., 1985; Allen et al., 1999; Tao et al., 2015).

During the SSW, vertical coupling covers not only the troposphere, but extends upward to the mesosphere. Mesospheric responses to the SSW are observed as enhancement in planetary wave amplitude, zonal wind reversal and significant air cooling (Shepherd et al., 2014; Zülicke and Becker, 2013; Stray et al., 2015; Zülicke et al., 2018), substantial depletions of the metal layers (Feng et al.,

2017; Gardner, 2018), mesosphere-to-stratosphere descent of trace species (Manney et al., 2009; Salmi et al., 2011). Mesospheric responses are also accompanied by vertical displacements of the stratopause (Chandran et al., 2011; Tomikawa et al., 2012; Limpasuvan et al., 2016; Orsolini et al., 2017).

Among trace gases, carbon monoxide (CO) is a good tracer of winter polar vortex dynamics in the upper stratosphere and mesosphere due to long photochemical lifetime (Solomon et al., 1985; Allen et al., 1999; Rinsland et al., 1999, Shepherd et al. 2014). The CO mixing ratio generally increases with height in the upper stratosphere and mesosphere and increases with latitude toward the winter pole. This is due to the mean meridional circulation which transports CO from the source region in the summer hemisphere and tropics to the extratropical winter mesosphere and stratosphere (Shepherd et al., 2014). Therefore, large abundances of CO appear in the winter polar regions under conditions of large-scale planetary wave activity. Downward meridional transport provides CO descent between mesosphere and stratosphere and this process is sensitive to the wave amplitudes increasing, in particular, during the SSW (Rinsland et al., 1999; Manney et al., 2009; Kvissel et al., 2012). At the NH midlatitudes, CO also exhibits significant variability during the periods of planetary wave activity in the SSW, when the polar vortex splits and displaces off the pole (Solomon et al., 1985; Allen et al., 1999).

Recent atmospheric models are being extended up to 80–150 km (de la Torre et al., 2012; Chandran and Collins, 2014; Shepherd at al., 2014; Limpasuvan et al., 2016; Newnham et al., 2016), for example, the Whole Atmosphere Community Climate Model (WACCM) by de la Torre et al. (2012) or the Canadian Middle Atmosphere Model (CMAM) by Shepherd at al. (2014). The reference data for the models are mainly obtained from observations of the radiation of the mesospheric ozone molecules, which allow robust measurements at altitudes up to of approximately 65 km (for example, Hagen et al., 2018). These data are generally consistent with the most commonly used ERA-Interim reanalysis products. However, there are still insufficient observations of middle atmospheric winds at altitudes between 60 and 85 km made with high vertical resolution to verify atmospheric models and possible long-term trends (Keuer et al., 2007; Rüfenacht et al., 2018). This altitude range with altitudinal temperature decrease and, therefore, with unstable atmosphere, locates below the winter mesopause region at 95–100 km (e.g. Xu et al., 2007) and plays a significant role in the mass and energy exchange in stratosphere–mesosphere coupling (Shepherd et al., 2014; Limpasuvan et al., 2016; Gardner, 2018).

Microwave radiometry is the ground-based technique that can provide vertical profiles of CO, H_2O and O_3 atmospheric gases and wind data in the upper stratosphere and mesosphere (Rüfenacht et al., 2012; Scheiben et al., 2012; Forkman et al., 2016). The upper stratosphere–mesosphere zonal winds at the 30–85 km altitude region can be measured using the Doppler shift between different observation directions in simultaneous measured spectra of transitions lines of carbon monoxide CO at 115.3 GHz

and ozone O_3 at 110.8 GHz (Rüfenacht et al., 2012; Forkman et al., 2016). Due to high altitude CO residence region, the simultaneous zonal wind measurements using both O_3 and CO provide independent data that extend the wind measurement from the stratospheric to mesospheric altitudes, respectively (Forkman et al., 2016; Piddyachiy et al., 2017).

The first ground-based microwave measurements of CO have been made in the 1970s and they have confirmed theoretical estimations of the vertical CO profile (Waters et al., 1976; Goldsmith et al., 1979). Since the 1990s, the ground-based microwave radiometers measuring CO have been installed in the Northern Hemisphere at high and middle latitudes to provide measurements on a regular basis. The microwave radiometers are operating in Onsala and Kiruna, Sweden, since 2008. The results are described in Hoffmann et al. (2011) and in Forkman et al. (2012). The microwave radiometer operated in Bern, Switzerland since 2010 aims to contribute to the significant gap that exists in the middle atmosphere between 40 and 70 km altitude for wind data (Rüfenacht et al., 2012). In the Arctic, the O_3, N_2O, HNO_3, and CO spectra were recorded using the Ground-Based Millimetre-wave Spectrometer GBMS (Muscari et al., 2007; Di Biagio et al., 2010).

Since 2014, the microwave measuring system for CO observations has been operated in Kharkiv, Ukraine (Piddyachiy et al., 2010; Piddyachiy et al., 2017). Microwave radiometer measurements of CO are used to retrieve mesospheric winds nearby the mesopause region (70–85 km). Methods deriving the wind speed from mesospheric CO measurements are based on the determination of the CO and O_3 lines emission Doppler shift (Eriksson et. al., 2011; Hagen et al., 2018).

Our observations in February 2018 have firstly recorded the mesospheric effects of a major sudden stratospheric warming at the mid-latitude station Kharkiv by the new microwave radiometer. In mid-February 2018, the stratospheric polar vortex in the Arctic splitted into two sub-vortices (Fig. 1), zonal wind reversed in the stratosphere–mesosphere from eastward to westward and warm air penetrated into the polar cap. This caused large-scale disturbances in the middle atmosphere of the polar and midlatitude regions. The major SSW in 2018 has not yet been widely discussed in publications (see e.g. Karpechko et al., 2018; Rao et al., 2018) and in this paper we give detailed description of the observed mesospheric CO and zonal wind variations.

In Sect. 2, the microwave radiometer and data processing software have been described shortly. The SSW event in February 2018 is considered in Sect. 3. The effects of the SSW on mid-latitude mesosphere–stratosphere conditions in the Ukraine longitudinal sector are presented in Sect. 4. Discussion is given in Section 5 followed by conclusion in Sect. 6.

Atmos. Chem. Phys. Discuss., https://doi.org/10.5194/acp-2018-1361
Manuscript under review for journal Atmos. Chem. Phys.
Discussion started: 7 February 2019

2 Data and methods

The microwave radiometer data set registered during 2017–2018 winter campaign in Kharkiv are used in this study to consider the winter 2018 sudden stratospheric warming effect on the mesosphere and upper stratosphere at this mid-latitude region. Since the ground-based microwave measurements are spatially limited by instrument coverage, data on air temperature, zonal wind, geopotential height were used from reanalyses and satellite databases to interpret CO profile and zonal wind microwave observations and to describe the SSW effects in the atmosphere of the surrounding region.

2.1 Microwave radiometer, method and midlatitude data description

The microwave radiometer (MWR) with high sensitivity, installed in mid-latitudes in Kharkiv (50.0°N, 36.3°E), Ukraine, is designed for continuous observations of the atmospheric CO profiles and winds in the mesosphere using emission lines at 115.3 GHz. The radiometer can continuously provide vertical profiles up to the mesopause region during day and night, even in cloud cover conditions (Hagen et al., 2018). The precipitation, such as strong rain or snow can prevent the radiometer measurements.

The receiver of the radiometer has the double-sideband noise temperature of 250 K at an ambient temperature of 10°C (Piddyachiy et al., 2010; Piddyachiy et al., 2017). The radiometer was tested during the 2014–2015 period in the carbon monoxide emission lines observations in the mesosphere over Kharkiv. These tests have shown the reliability of the receiver system. More detail on the microwave radiometer design and characteristics are given in (Piddyachiy et al., 2017). Since 2015, the radiometer is used for continuous microwave measurements of carbon monoxide profiles and mesosphere wind investigations. The first observations of the atmospheric carbon monoxide spectral lines over Kharkiv have confirmed seasonal variations in the CO abundance (Piddyachiy et al., 2017). The radiometer with the double-side band mode allows retrieving the wind speed from the Doppler shift of the CO line emission at the 115.3 GHz. Two methods are used to determine wind speed. The first, the observed line shape is fitted by a Voigt profile followed by search the center frequency (Piddyachiy et al., 2017). The second, a radiative transfer calculations for horizontally layered atmosphere are used to determine the wind profiles with the Qpack package, version 1.0.93 (Eriksson et al., 2005; Eriksson et. al., 2011), which is specifically designed to work with the forward model of the Atmospheric Radiative Transfer Simulator ARTS (Buehler et al., 2018; http://www.radiativetransfer.org/). The results obtained by both methods were almost the same within the error limits. In this article, we use the averaged values of the zonal wind speed for altitudes of 70–85 km.

The CO molecules vertical profiles from the measured spectra taken from ground-based microwave instrument in Kharkiv and the zonal winds in the upper stratosphere–mesosphere region were retrieved similar to Rüfenacht et al. (2012). Time interval January 1 – March 31, 2018 including the SSW 2018 event is considered in this paper.

2.2 Data from other sources

In this study, daily datasets from ERA-Interim global atmospheric reanalysis of European Centre for Medium-Range Weather Forecast (ECMWF; Dee et al., 2011) were downloaded from (https://www.ecmwf.int/en/forecasts/datasets/archive-datasets/reanalysis-datasets/era-interim) have been used for comparison with microwave radiometer observations. Horizontal resolution (longitude/latitude) in the ERA-Interim database is selected as 0.75°/0.75°. The ERA-Interim data were used to create temperature and zonal wind velocity profiles from surface up to 0.01 hPa, and to calculate geopotential height at the stratospheric pressure levels, in order to compare with the data measured over Kharkiv site. The data of air temperature, zonal wind, and geopotential height were used also from the NCEP–NCAR reanalysis data (Kalnay et al., 1996; https://www.esrl.noaa.gov/psd/cgi-bin/data/getpage.pl). Aura Microwave Limb Sounder (MLS) measurements of the air temperature were analyzed as well (Xu et al., 2009). The MLS data are presented for 55 vertical layers, in particular layers 43-49 cover pressure levels from 0.1 hPa to 0.001 hPa (64–96 km approximately). The vertical resolution in this altitudinal range is about 5 km. ERA-Interim data include 60 vertical layers from the surface up to 0.1 hPa only (https://mls.jpl.nasa.gov/data/readers.php).

3 Northern Hemisphere sudden stratospheric warming in February 2018

General tendency in the winter polar region is descending motion throughout the mesosphere and stratosphere (Orsolini et al., 2010; Chandran and Collins, 2014; Limpasuvan et al., 2016; Zülicke et al., 2018). From the Aura MLS vertical profiles, sequence of alternating cool and warm anomalies descending over the polar cap was observed in winter 2017–2018 (Fig. 2a). The SSW event in February 2018 is presented here by enhanced warming in the stratosphere and cooling in the mesosphere (arrow in Fig. 2a). However, this modification was preceded by mesosphere warming and stratosphere cooling in January 2018 (Fig. 2a). Both these anomalies in January were formed under influence of the large amplitude planetary waves (Fig. 2d) and, probably, gravity waves, which loose

stability and dissipate in the stratosphere and mesosphere (Pedatella et al., 2018). The temperature anomalies were enhanced in February being descending (arrow in Fig. 2a).

The major sudden stratospheric warming has been started with the zonal wind reverse and air temperature increase in the upper–middle stratosphere over polar cap near 10 February 2018 (vertical line in Fig. 2b and 2c, respectively). This is close to the SSW timing in Rao et al. (2018), where the SSW onset date is 11 February. As seen from Fig. 2d, increasing wave-1 amplitude contributed to the polar vortex destabilization during the second half of January–early February producing zonal wind and temperature oscillations in the upper stratosphere (Fig. 2b and 2c). These oscillations are usually associated with the planetary wave propagated in the stratosphere and mesosphere (Limpasuvan et al., 2016; Rüfenacht et al., 2016). As noted in an earlier study (Manney et al., 2009), wave-1 amplitudes were larger also prior to the SSW 2009, suggesting a larger role of preconditioning. During 10–15 February, the easterly zonal wind anomaly at the stratopause (about 1 hPa, ~50 km) increased to –60 m s^{-1} (Fig. 2b). At the same time, the warming in the polar region with the largest temperature anomaly of about 20°C was observed in the middle stratosphere (around 10 hPa, Fig. 2c).

The wave-2 impulse on 10 February (dashed curve in Fig. 2c) was responsible for the polar vortex split in the two parts (Fig. 1 in Sect. 1). This indicates that the SSW in February 2018 refers to the wave-2 forcing, similarly to the SSW 2009 (Manney et al., 2009; Yuan et al., 2012). Note that wave-1 and wave-2 amplitudes varied approximately in antiphase in January and February (Fig. 2d) and contributed to vortex displacement and vortex split, respectively. Similar anti-correlated amplitudes of wave-1 and wave-2 in the stratosphere during the 2009 SSW were noted by Yuan et al. (2012). Since the wave-1 peak in mid-February was of the same amplitude as the wave-2 peak on 10 February (~1000 m, Fig. 2c), both wave numbers participated in the middle–upper stratosphere warming.

The development of the major SSW is well described by the Eliassen–Palm flux vector, which is a measure of the heat and momentum fluxes transferred by planetary waves from the troposphere to the stratosphere (Matsuno, 1971; de la Torre et al., 2012; Chandran and Collins, 2014). The changing wave activity in February 2018 can be seen from EP-flux in the NCEP–NCAR reanalysis at https://www.esrl.noaa.gov/psd/data/epflux/ (Fig. 3) that follows the changing wave amplitudes in Fig. 2d.

An intense EP-flux since February 6 (Fig. 3b and 3c) initiated the vortex split on February 10 (Fig. 1c). The EP-flux vector was in prevailing upward direction covering the NH extratropics till February 20–21, when equatorward EP-flux became almost horizontal and reached the tropics (Fig. 3d). Note that on February 7–8, the EP flux vectors reached the equator (not shown), in consistency with easterly phase of the quasi-biennial oscillation (QBO) in February 2018 (https://www.esrl.noaa.gov/psd/data/correlation/qbo.data). In these conditions in the tropical stratosphere, waves originating at higher latitudes propagate across the equator (Chandran and Collins,

2014). The EP flux weakened sharply in late February (Fig. 3f) in correspondence with wave amplitude decrease (Fig. 2d) that favored start of the SSW recovery phase.

4 The local SSW effects over the mid-latitude station

Local variability in the conditions of the atmosphere during the microwave measurements in January–March 2018 at Kharkiv (50°N, 35°E) is shown in Fig. 4 and Fig. 5. The sharp changes occurred in the 20-day interval coinciding with the SSW event 2018 from February 10 to March 1, as indicated by red vertical lines in Fig. 4 and Fig. 5. This is a time, when the polar vortex divided into two parts producing two smaller vortices over North America and Eurasia (Fig. 1).

The CO molecule volume mixing ratio (WMR) near the mesopause at 75–80 km decreased from 10 ppmv of background level to 4 ppmv on 19–21 February (Fig. 4a), when the sharp vertical CO gradient at the lower edge of the CO layer near about 6 ppmv elevated by about 8 km (between 75 km and 83 km, thick part of the white curve in Fig. 4a). For comparison, the pre- and post-SSW vertical variations of the 6-ppmv level were observed in a range 2–3 km (thin parts of the white curve in Fig. 4a). We take here the 6-ppmv level as a conditional lower edge of the CO layer, since the CO gradients sharply increases from 0.2–0.3 ppmv km^{-1} in a 10-km layer below to 0.6–0.8 ppmv km^{-1} in a 10-km layer above (below and above the white curve in Fig. 4a). The similar gradient change is characteristic of the mesospheric CO profiles in boreal winter from ground-based and satellite observations (Koo et al., 2017, their Fig. 4; Rayan et al., 2017, their Fig. 5).

The reversal of the local zonal wind estimated from the CO measurements at the Kharkiv microwave radiometer site nearby the mesopause region was observed. The averaged wind velocity in the altitude range 70–85 km changed between 10 m s^{-1} and –10 m s^{-1} around 10 February (Fig. 4b). After the active phase of the SSW, zonal wind returns to eastward direction and enhances to 20 m s^{-1} reaching the highest velocity observed in January–March (Fig. 4b). This zonal wind peak in early March is accompanied by the CO peak at 18 ppmv that is also the highest CO abundance over January–March (Fig. 4a). During the SSW event, local zonal wind over the station became easterly between the lower stratosphere and lower mesosphere (–30 m s^{-1} up to –40 m s^{-1}, white contours in Fig. 4c). Note that westerly zonal wind at the stratopause level (~ 50 km) in January 2018 (mid-winter, the pre-SSW conditions) sometimes increased to more than 100 m s^{-1} (black contours in Fig. 4c). Due to the wave activity in January–February, the air temperature maximum at the stratopause was likewise unstable and it slowly recovered in March (Fig. 4d).

The SSW effects in February 2018 were the strongest in polar region and were also clearly observed in the middle NH latitudes as noted above. Manifestations of the midlatitude anomalies

during the SSW are seen from geopotential height (Z) variability in Fig. 5. The Z anomalies extend from the polar to subtropical latitudes in the upper and middle stratosphere (at 1 hPa and 10 hPa in Fig. 5a and 5b, respectively). During the SSW (red vertical lines in Fig. 5), the geopotential height levels rapidly rise not only relative to the pre-SSW levels (by 4 km in high latitudes and by 1 km at 50°N), but also relative to the tropical geopotential height levels. This Z gradient between the pole and tropics is reversed to that observed in the pre-SSW period. That displays meridional temperature gradient reversal in the stratosphere during the SSW development (Butler et al., 2015) and is not fully restored after the event (compare the Z levels in January and March in Fig. 5). The midlatitude SSW effects are known from many event analyses and in most cases they are associated with zonal asymmetry and polar vortex split and displacements relative to the pole (Solomon et al., 1985; Allen et al., 1999; Yuan et al., 2012; Chandran and Collins, 2014).

Since Fig. 5 represents a relatively narrow longitude interval (30–40°E), the vortex location and its motions under influence of the wave-1 and wave-2 amplitude variations (Fig. 2d), are accompanied by concurrent displacements of midlatitude air mass that is observed in the local variability of the atmospheric parameters. At the upper stratosphere levels, the general Z increase during the SSW relates to the stratopause elevation. At the same time, the vortex split, its meridional and zonal migrations lead to the geopotential height oscillations. This is seen from the Z peaks in Fig. 5a and 5b that appeared not only in the polar region, but also in the midlatitudes (black curve in Fig. 5b). Similar oscillations reach the midlatitude mesosphere and are reflected in the enhanced variations of the CO vertical profile over the Kharkiv site (thick part of the white curve in Fig. 4a). The dominated 5–8 day periods of the oscillations are seen from the ridge and trough sequence along the white curve in Fig. 4a. This corresponds to the periodicity range in planetary waves propagated in the stratosphere and mesosphere with the periods 5–12 days (Limpasuvan et al., 2016) or atmospheric normal modes with periods 5, 10 and 16 days (Rüfenacht et al., 2016).

The SSW effects in geopotential height in February weaken in the lower stratosphere (Fig. 5c), in agreement with zonal mean zonal wind U and zonal mean temperature T variations as shown in Fig. 6. Figure 6 presents time–altitude sections at individual latitudes for February 2018 covered the attitude range above the tropopause up to the stratopause. Zonal wind reversal is seen around 10 February from polar to middle latitudes (90–50°N, contour –10 m s^{-1} in Fig. 6a–6d) and easterly velocities exhibit two–three consecutive peaks during the SSW. These peaks are similar to 5–8 day oscillations observed in other variables (Fig. 4 and Fig. 5) and associated with the polar vortex split and two sub-vortices migrations due to changing wave activity noted above.

Zonal wind reversal extends through the stratosphere between the stratopause and tropopause in the polar vortex region (80°N and 70°N, Fig. 6a and 6b). However, reverse process occurs only

between the middle and upper stratosphere at the vortex edge region (60°N, Fig. 6c), and weakens at the middle latitude 50°N (Fig. 6d). This shows deeper penetration of easterly wind inside the polar vortex (80°N and 70°N) than outside (50°N and 40°N). Note that the meridional tendency seen from the sequence of individual latitudinal circles in Fig. 6 would be smoothed out or completely disappeared when averaged over a wide mid-latitude (40–60°N) or high-latitude (60–80°N) zone.

Simultaneously, rapid warming in the polar stratosphere is observed since 10 February (Fig. 6f and 6g). The stratopause temperature maximum in the polar region descends in the middle of February (contour –30°C in Fig. 6f and 6g) and disappears later, leading to a nearly isothermal middle atmosphere at about –35°C (see also Fig. 4d), in agreement with other observations (e.g. Manney et al., 2009). As known, the SSW events are accompanied by stratopause descent to 30–40 km, by stratopause breakdown and subsequent reformation at very high altitudes of about 70–80 km (Manney et al., 2009; Chandran et al., 2011; Limpasuvan et al,. 2016; Orsolini et al., 2017). Because our results in Fig. 6 are limited at the upper level by 1 hPa at about 48 km altitude, the stratopause behaviour at mesospheric altitudes could not be revealed. Stratopause descent, disappearing and recovery in February–March 2018 are clearly observed also from the local midlatitude data in Fig. 4d.

Warming penetrates less deeply at lower latitudes (compare contour –50°C in Fig. 6f–6j). At 40°N, the zonally averaged T is relatively stable in vertical distribution before, during and after the SSW (Fig. 6j) and only weak anomaly appears in zonal wind (Fig. 6e). Steady temperature maximum at about 1–2 hPa (contour –30°C in Fig. 6j) demonstrates undisturbed stratopause at 40°N throughout February. Therefore, the SSW influence on the midlatitude stratosphere in February 2018 weakened significantly at 40°N.

5 Discussion

The observations of the major SSW effects in February 2018 in the NH midlatitude mesosphere by microwave radiometer at the Kharkiv site, Northern Ukraine (50.0°N, 36.3°E), have been provided. Using the CO molecule as tracer, westward mesospheric wind reverse at 70–85 km altitudes, below the winter mesopause region, has been detected. The wind speed data have been retrieved from the Doppler shift of the CO 115.27 GHz emission measured by microwave radiometer. A few ground-based observations in the mesosphere by the same method have been undertaken at midlatitudes (Sect. 1). The microwave radiometer at Kharkiv with 115 GHz frequency allows reconstructing the CO profiles and zonal wind from observation with one day time resolution. The zonal wind and CO profile variability during the major SSW was compared with daily zonal wind, temperature and geopotential

348 height datasets from the ERA-Interim and NCEP–NCAR reanalyzes. The SSW started with the polar
349 vortex split around 10 February (Fig. 1), zonal wind reverse in the mesosphere (Fig. 4b) and
350 stratosphere (Fig. 2a, Fig. 4c and Fig. 6a–6d) and enhanced stratosphere warming (Fig. 2a and 2c) and
351 mesosphere cooling (Fig. 2a).
352 Among the most striking SSW manifestations over the midlatitude station in February 2018, there
353 were (i) zonal wind reversal throughout the mesosphere–stratosphere with weakened easterly anomaly
354 between the polar and middle latitudes, (ii) oscillations in the vertical CO profile, zonal wind and
355 geopotential height, (iii) stratopause disappearance and (iv) strong mesospheric CO and westerly peaks
356 at the start of the SSW recovery phase.
357 As noted in Sect. 1, CO abundance in the extratropical mesosphere increases in winter season due
358 to meridional and downward transport. CO accumulation results in formation of the CO layer with
359 sharp vertical gradient at its lower edge (Solomon et al., 1985; Shepherd et al., 2014). In Sect. 4, based
360 on the microwave radiometer observations, we have defined the lower CO edge at 6 ppmv and this
361 edge uplifted during the SSW by about 8 km (between 75 km and 83 km, thick part of the white curve
362 in Fig. 4a). This uplifting noticeably stands out against the pre- and post-SSW variations of the 6-ppmv
363 level occurring within 2–3 km (Fig. 4a). Mesospheric CO profile uplifting is usually associated with
364 the stratopause elevation during the SSW, when air, poor in CO, enters the mesospheric CO layer from
365 below (Kvissel et al., 2012; Shepherd et al., 2014). Similar ascending motions in the stratopause and
366 mesopause regions were observed in the 2013 SSW from nitric oxide (NO) and showed that the NO
367 contours deflected upwards throughout the mesosphere (Orsolini et al., 2017).
368 The stratopause elevation during the SSW is more pronounced in the polar region and the results
369 of Fig. 5 is evidence of midlatitude manifestation of similar processes. Geopotential heights Z in time–
370 latitude section at 1 hPa and 10 hPa in Fig. 5a and 5b show strongly increased levels poleward of 70°N
371 and moderately increased levels in the northern midlatitude (particularly, near the black line at 50°N).
372 This Z increase at 1 hPa is directly related to the stratopause elevation and the lower CO edge uplift in
373 Fig. 4a. As noted in Sect. 4, the polar geopotential height Z levels become higher than the tropical ones
374 that displays meridional temperature gradient reversal in the stratosphere during the SSW development
375 (Butler et al., 2015).
376 Elevation of the lower CO edge maximizes on 18–20 February (Fig. 4a), up to 10 days after the
377 zonal wind reversal in the stratosphere (Fig. 4c) and mesosphere (Fig. 4b). Similar time lag in the
378 planetary wave activity in the mesosphere was noted recently. A significant enhancement in wave-1
379 and wave-2 amplitudes near 95 km was found to occur after the wind reversed at 50 km, with
380 amplitudes maximizing approximately 5 days after the onset of the wind reversal (Stray et al., 2015).
381 The effects of zonal asymmetry can also play a role in the appearance of regional low-CO
382 anomaly. Large scale planetary waves can displace parcels of air meridionally over the large distance

at particular longitudes and any species having a latitude gradient should be influenced by such transport process; this suggests that latitudinal displacements due to wave effects should dramatically affect their local densities (Solomon et al., 1985). Therefore, polar vortex displacement can be an additional cause of the CO decrease and CO profile uplift over Kharkiv in February 2018 in Fig. 4a. As seen from Fig. 1, the vortex was shifted off pole to the North America sector (along meridian ~90°W) under the wave-1 influence and the increased wave-1 amplitude persisted in January and February (Fig. 2d). Midlatitude air at opposite eastern longitudes approached the pole moving the CO-poor parcels to the higher latitudes. As known, the strong vertical CO gradient in the winter mesosphere is found at higher altitudes in the tropics than in the extratropics (Solomon et al., 1985; Allen et al., 1999; Garcia et al., 2014). Then, poleward displacement of the low-latitude air masses is accompanied by the CO abundance decrease and strong vertical CO gradient elevation at the higher latitudes, as it is observed in Fig. 4a.

A similar wave-1 effect was observed during the 2003–2004 Arctic warming (Funke et al., 2009): the vortex has shifted from the pole toward the western sector and mid-latitude air poor in CO filled the eastern sector (0–90°E) over 50–80°N and even over the pole. Influence of meridionally transported midlatitude low-CO air on the observed local negative anomalies of CO at the higher latitudes was noted in Solomon et al. (1985) and Shepherd et al. (2014). Typically, wave 1 influence on the polar vortex displacement is associated with forming a winter midlatitude anticyclone that pushes the vortex off the pole (Solomon et al., 1985; Allen e al., 1999; Kvissel et al., 2012).

Note, that the large wave-1 amplitude in the middle stratosphere in January 2018 (500–1500 m, Fig. 2d) indicates one of possible sources of the mesospheric warming in January 2018 (Fig. 2a). The descent of warm mesospheric anomaly in the polar region, where the relatively homogeneous conditions persist due to strong winter westerly jet (~50–100 m s^{-1}) circulating in the polar night, looks regular and continues during January–March down to the lower stratosphere (Fig. 2a). The mesosphere warming in January was again replaced by strong cooling in active phase of SSW since February 10 creating alternating altitudinal sequence of warm and cool anomalies extended from the lower stratosphere up to thermosphere (Fig. 2a) in consistency with many observations (Zhou et al., 2002; Orsolini et al., 2010; Shepherd et al., 2014; de Wit et al., 2014; Zülicke et al., 2018).

Variations in wave amplitudes (Fig. 2d) are a possible cause of the oscillations in CO, zonal wind and geopotential height described in Sect. 4. These 5–8 day oscillations are observed not only from local data (Fig. 4a and Fig. 5), but also from zonal means (Fig. 6a–6c), in confirming the existence of a large-scale process. Similar periodicity is observed in January–February 2018 from eddy heat flux at the 50-hPa level (not shown; see e.g. https://acd-ext.gsfc.nasa.gov/Data_services/met/ann_data.html). The simulations made by Limpasuvan et al. (2016) shows that PW forcing by westward propagating waves with zonal wave number 1 dominates above 70 km in the winter hemisphere. Our results

indicate important role of wave 2 in the SSW forcing in February 2018 (Fig. 4), in consistency with previous studies of the vortex splitting events in the SSW. The role of planetary wave spectrum in enhanced variability of vertical CO profile during the SSW deserves further analysis using observational and model data. In March 2018, after the SSW, vertical CO profile along with the temperature maximum at the stratopause at about 50–60 km were re-established (Fig. 4a and 4d, respectively) according to the recovery phase following the SSW (Shepherd et al., 2014; Limpasuvan et al., 2016).

The SSW recovery phase in the mesosphere started with the short-term but anomalously high peaks in the local CO and westerly wind in early March (Fig. 4a and 4b). These peaks reached the highest values in daily variations of CO and zonal wind over the three months of the observations (January–March). Note that the warm local anomaly ~10K appeared in the mesosphere at 70–90 km in the early March (arrow in Fig. 7). By analogy with the low-CO episode in February discussed above, the high-CO peak in early March 2018 could be caused by a combination of processes: (a) re-establishment of the westerly and midlatitude anticyclone weakening leading to (b) displacement of polar air mass over the observation site toward equator that brings higher CO level into the midlatitudes and (c) in contrast to ascent motions in the active phase of the SSW, descent of CO-rich air takes place in the recovery phase. Enhanced mesospheric descent and peak in westerly velocity at the start of recovery phase were noted in Kvissel et al. (2012) Shepherd et al. (2014) and Orsolini at al. (2017).

On the seasonal time scale, the lower CO edge at 6 ppmv gradually rises in January–March 2018 by approximately 3 km (dashed white line in Fig. 4a). This seasonal tendency can be explained by its annual cycle, considering that the strong vertical CO gradient in the NH mesosphere takes the lowest altitudes in winter and the highest altitudes in summer (Garcia et al., 2014).

6 Conclusions

The impact of a major sudden stratospheric warming (SSW) in February 2018 on the mid-latitude mesosphere was investigated using microwave radiometer measurements in Kharkiv, Ukraine (50.0°N, 36.3°E). The zonal wind reversal during the SSW has been revealed below the winter mesopause region at 70–85 km altitudes during the SSW using the carbon monoxide profiles. The reverse of the mesospheric westerly from about 10 m s^{-1} to easterly wind about –10 m s^{-1} around 10 February has been registered. The data from the ERA-Interim and NCEP–NCAR reanalyses and the Aura MLS temperature profiles have been used for analysis of stratosphere–mesosphere behavior under the SSW conditions. Our local microwave observations in the NH midlatitude combined with the reanalysis data

show wide ranges of daily variability in CO, zonal wind, temperature and geopotential height in the mesosphere and stratosphere during the SSW 2018.

Among the most striking manifestations of the SSW 2018 are the following: (i) oscillations in the vertical CO profile, zonal wind and geopotential height, (ii) stratopause disappearance at the SSW onset (iii) strong CO and westerly peaks at the start of the SSW recovery phase, and (iv) progressively weakened easterly wind and temperature anomalies in the stratosphere between the polar and middle latitudes, almost disappearing at 40°N. The observed CO variability can be explained by vertical and horizontal air mass redistribution due to planetary wave activity with replacement of the CO-rich air by CO-poor air and vice versa, in agreement with other studies. Microwave observations show that sharp altitudinal CO gradient below the mesopause could be used to define the lower edge of the CO layer and to evaluate oscillation and significant elevation of the lower CO edge during the SSW and its trend on seasonal time scale.

The presented results of microwave measurements of CO and zonal wind in the midlatitude mesosphere at 70–85 km altitudes, which still not adequately covered by ground-based observations (Rüfenacht et al., 2018), are suitable for evaluating and potentially improving atmospheric models. Simulations show that PW forcing by westward propagating waves with zonal wave number 1 dominates above 70 km in the winter hemisphere (Limpasuvan et al., 2016). Consistent with previous studies of the vortex splitting events during SSWs, our results indicate the important role of wave 2 in the dynamics of the February 2018 SSW. In reanalysis data sets, the low-order zonal waves are well-resolved (Lu et al., 2015) but are usually represented in the wind field of the upper stratosphere and lower mesosphere through the quasi-geostrophic approximation using satellite radiance measurements (e.g. Duruisseau et al., 2017). The validity of the quasi-geostrophic approximation can break down in strong wave events (Ern et al., 2016; Martineau et al., 2018). Wind measurements using the CO layer provides a further means to evaluate the validity of the modelled winds. Furthermore, by combining the measurements with ray tracing of gravity wave propagation (e.g. Kogure et al., 2018), this type of measurement may provide particular insights into wave-mean flow interactions, particularly where local temperature inversions alter gravity wave filtering (Hocke et al., 2018; Fritts et al., 2018). Our observation of variability of the CO layer during the SSW deserves further study, particularly in relation to the implications for modelling of wave dynamics and vertical coupling (Ern et al., 2016; Martineau et al., 2018) and chemical processes (Garcia et al., 2014) in the mesosphere.

Conflict of Interest. The authors declare that the research was conducted in the absence of any commercial or financial relationships that could be construed as a potential conflict of interest.

Author contributions. GM coordinated and led the efforts for this manuscript. VS initiated the microwave measurements during the SSW event in Kharkiv. VS, DS, VM and AA developed equipment and provided microwave measurements with data processing by AP and DS. GM, VS, YW, OE, AK, and AG analyzed the results and provided interpretation. GM, VS, OE, AK, and WH wrote the paper with input from all authors.

Acknowledgements. This work was supported in part by the Institute of Radio Astronomy of the National Academy of Sciences of Ukraine; by Taras Shevchenko National University of Kyiv, project 19BF051-08; by the College of Physics, International Center of Future Science, Jilin University, China. The microwave radiometer data have been processed using ARTS and Qpack software packages (http://www.radiativetransfer.org/). NCEP–NCAR reanalysis data were provided by the NOAA/OAR/ESRL PSD, Boulder, Colorado, USA, from their Web site at http://www.esrl.noaa.gov/psd/. Daily datasets from ERA-Interim reanalysis of European Centre for Medium-Range Weather Forecast (ECMWF) were downloaded from https://www.ecmwf.int/en/forecasts/datasets/archive-datasets/reanalysis-datasets/era-interim. The Aura Microwave Limb Sounder (MLS) measurements of the air temperature were used from https://mls.jpl.nasa.gov/data/readers.php.

References

Alexander, S. P. and Shepherd, M. G.: Planetary wave activity in the polar lower stratosphere, Atmos. Chem. Phys., 10, 707–718, https://doi.org/10.5194/acp-10-707-2010, 2010.

Allen, D. R., Stanford, J. L., López-Valverde, M. A., Nakamura, N., Lary, D. J., Douglass, A. R., Cerniglia, M. C., Remedios, J. J., and Taylor F. W.: Observations of middle atmosphere CO from the UARS ISAMS during the early northern winter 1991/92, J. Atmos. Sci., 56, 563–583, 1999.

Baldwin, M. P. and Dunkerton, T. J.: Stratospheric harbingers of anomalous weather regimes, Science, 294, 581–584, doi:10.1126/science.1063315, 2001.

Buehler, S. A., Mendrok, J., Eriksson, P., Perrin, A., Larsson, R., and Lemke, O.: ARTS, the atmospheric radiative transfer simulator – version 2.2, the planetary toolbox edition, Geosci. Model Dev., 11, 1537–1556, doi:10.5194/gmd-11-1537-2018, 2018.

Butler, A. H. and Gerber, E.P. Optimizing the definition of a sudden stratospheric warming, J. Climate, 31, 2337–2344, doi:10.1175/JCLI-D-17-0648.1, 2018.

522 Butler, A. H., Seidel, D. J., Hardiman, S. C., Butchart, N., Birner, T., and Match, A.: Defining sudden
523 stratospheric warmings, Bull. Amer. Meteor. Soc., 96, 1913–1928, doi:10.1175/bams-d-13-
524 00173.1, 2015.
525 Butler, A. H., Sjoberg, J. P., Seidel, D. J., and Rosenlof, K. H.: A sudden stratospheric warming
526 compendium, Earth Syst. Sci. Data, 9, 63–76, doi:10.5194/essd-9-63-2017, 2017.
527 Chandran, A. and Collins, R. L.: Stratospheric sudden warming effects on winds and temperature in
528 the middle atmosphere at middle and low latitudes: a study using WACCM, Ann. Geophys., 32,
529 859–874, doi:10.5194/angeo-32-859-2014, 2014.
530 Chandran, A., Collins, R. L., Garcia, R. R., and Marsh, D. R.: A case study of an elevated stratopause
531 generated in the Whole Atmosphere Community Climate Model, Geophys. Res. Lett., 38, L08804,
532 doi:10.1029/2010GL046566, 2011.
533 Dee, D. P., Uppala, S. M., Simmons, A. J., Berrisford, P., Poli, P., Kobayashi, S., Andrae, U.,
534 Balmaseda, M. A., Balsamo, G., Bauer, P., Bechtold, P., Beljaars, A., van de Berg, L., Bidlot, J.,
535 Bormann, N., Delsol, C., Dragani, R., Fuentes, M., Geer, A. J., Haimberger, L., Healy, S. B.,
536 Hersbach, H., Hólm, E. V., Isaksen, L., Kallberg, P., Köhler, M., Matricardi, M., McNally, A. P.,
537 Monge-Sanz, B. M., Morcrette, J.-J., Park, B. K., Peubey, C., de Rosnay, P., Tavolato, C., Thépaut,
538 J.-N., and Vitart, F.: The ERA-Interim reanalysis: configuration and performance of the data
539 assimilation system, Q. J. Roy. Meteor. Soc., 137, 553–597, doi:10.1002/qj.828, 2011.
540 de la Torre, L., Garcia, R. R., Barriopedro, D., and Chandran, A.: Climatology and characteristics of
541 stratospheric sudden warmings in the Whole Atmosphere Community Climate Model, J. Geophys.
542 Res., 117, D04110, doi:10.1029/2011JD016840, 2012.
543 de Wit, R. J., Hibbins, R. E., Espy, P. J., Orsolini, Y. J., Limpasuvan, V., and Kinnison, D. E.:
544 Observations of gravity wave forcing of the mesopause region during the January 2013 major
545 Sudden Stratospheric Warming, Geophys. Res. Lett., 41, 4745–4752, doi:10.1002/2014GL060501,
546 2014.
547 Di Biagio, C., Muscari, G., di Sarra, A., de Zafra, R. L., Eriksen, P., Fiocco, G., Fiorucci, I., and Fuà,
548 D.: Evolution of temperature, O_3, CO, and N_2O profiles during the exceptional 2009 Arctic major
549 stratospheric warming as observed by lidar and millimeter wave spectroscopy at Thule (76.5N,
550 68.8W), Greenland, J. Geophys. Res., 115, D24315, doi:10.1029/2010JD014070, 2010.
551 Duruisseau, F., Huret, N., Andral, A., and Camy-Peyret, C.: Assessment of the ERA-Interim winds
552 using high-altitude stratospheric balloons. J. Atmos. Sci., 74, 2065–2080,
553 https://doi.org/10.1175/JAS-D-16-0137.1, 2017.
554 Eriksson, P., Buehler, S. A., Davis, C. P., Emde, C., and Lemke, O.: ARTS, the atmospheric radiative
555 transfer simulator, version 2, J. Quant. Spectrosc. Radiat. Transfer, 112, 1551–1558, doi:
556 10.1016/j.jqsrt.2011.03.001, 2011.

Eriksson, P., Jiménez, C., and Buehler, S. A.: Qpack, a tool for instrument simulation and retrieval work, J. Quant. Spectrosc. Radiat. Transfer, 91, 47–64, doi: 10.1016/j.jqsrt.2004.05.050, 2005.

Ern, M., Trinh, Q. T., Kaufmann, M., Krisch, I., Preusse, P., Ungermann, J., Zhu, Y., Gille, J. C., Mlynczak, M. G., Russell III, J. M., Schwartz, M. J., and Riese, M.: Satellite observations of middle atmosphere gravity wave absolute momentum flux and of its vertical gradient during recent stratospheric warmings, Atmos. Chem. Phys., 16, 9983-10019, https://doi.org/10.5194/acp-16-9983-2016, 2016.

Feng, W., Kaifler, B., Marsh, D. R., Höffner, J., Hoppe, U. P., Williams, B. P., and Plane J. M. C.: Impacts of a sudden stratospheric warming on the mesospheric metal layers, J. Atmos. Solar-Terr. Phys., 162, 162–171, 2017.

Fritts, D. C., Laughman, B., Wang, L., Lund, T. S., and Collins, R. L.: Gravity wave dynamics in a mesospheric inversion layer: 1. Reflection, trapping, and instability dynamics. Journal of Geophysical Research: Atmospheres, 123, 626–648. https://doi.org/10.1002/2017JD027440, 2018.

Forkman, P., Christensen, O. M., Eriksson, P., Urban, J., and Funke, B.: Six years of mesospheric CO estimated from ground-based frequency-switched microwave radiometry at 57° N compared with satellite instruments, Atmos. Meas. Tech., 5, 2827–2841, doi: 10.5194/amt-5-2827-2012, 2012.

Forkman, P., Christensen, O. M., Eriksson, P., Billade, B., Vassilev, V., and Shulga, V. M.: A compact receiver system for simultaneous measurements of mesospheric CO and O_3, Geosci. Instrum. Method. Data Syst., 5, 27–44, doi:10.5194/gi-5-27-2016, 2016.

Funke, B., López-Puertas, M., García-Comas, M., Stiller, G. P., von Clarmann, T., Höpfner, M., Glatthor, N., Grabowski, U., Kellmann, S., and Linden, A.: Carbon monoxide distributions from the upper troposphere to the mesosphere inferred from 4.7μm non-local thermal equilibrium emissions measured by MIPAS on Envisat, Atmos. Chem. Phys., 9, 2387–2411, 2009.

Garcia, R. R., López-Puertas, M., Funke, B., Marsh, D. R., Kinnison, D. E., Smith, A. K., and González-Galindo, F.: On the distribution of CO_2 and CO in the mesosphere and lower thermosphere, J. Geophys. Res.-Atmos., 119, 5700–5718, doi:10.1002/2013JD021208, 2014.

Gardner, C. S.: Role of wave-induced diffusion and energy flux in the vertical transport of atmospheric constituents in the mesopause region, J. Geophys. Res.-Atmos., 123, 6581–6604, https://doi.org/10.1029/2018JD028359, 2018.

Goldsmith, P. F., Litvak, M. M., Plambeck, R. L., and Williams, D. R.: Carbon monoxide mixing ratios in the mesosphere derived from ground-based microwave measurements, J. Geophys. Res., 84, 416–418, 1979.

Hagen, J., Murk, A., Rüfenacht, R., Khaykin, S., Hauchecorne, A., and Kämpfer, N.: WIRA-C: a compact 142-GHz-radiometer for continuous middle-atmospheric wind measurements. Atmos. Meas. Tech., 11, 5007–5024, doi: 10.5194/amt-11-5007-2018, 2018.

592 Hocke, K., Lainer, M., Bernet, L., and Kämpfer, N.: Mesospheric inversion layers at mid-latitudes and
593 coincident changes of ozone, water vapour and horizontal wind in the Middle Atmosphere.
594 Atmosphere, 9, 171, https://doi.org/10.3390/atmos9050171, 2018.
595 Hoffmann, C. G., Raffalski, U., Palm, M., Funke, B., Golchert, S. H. W., Hochschild, G., and Notholt,
596 J.: Observation of strato-mesospheric CO above Kiruna with ground-based microwave radiometry
597 – retrieval and satellite comparison, Atmos. Meas. Tech., 4, 2389–2408,
598 https://doi.org/10.5194/amt-4-2389-2011, 2011.
599 Kalnay, E., Kanamitsu, M., Kistler, R., Collins, W., Deaven, D., Gandin, L., Iredell, M., Saha, S.,
600 White, G., Woollen, J., Zhu, Y., Chelliah, M., Ebisuzaki, W., Higgins, W., Janowiak, J., Mo, K. C.,
601 Ropelewski, C., Wang, J., Leetmaa, A., Reynolds, R., Jenne, R., and Joseph, D.: The NCEP–
602 NCAR 40-year Reanalysis Project, B. Am. Meteorol. Soc., 77, 1057–1072, doi:10.1175/1520-
603 0477(1996)077<0437:TNYRP>2.0.CO; 2, 1996.
604 Karpechko, A. Yu., Charlton-Perez, A., Balmaseda, M., Tyrrell N., and Vitart, F.: Predicting sudden
605 stratospheric warming 2018 and its climate impacts with a multi-model ensemble, Geophys. Res.
606 Lett., available at: https://doi.org/10.1029/2018GL081091, 2018.
607 Keuer, D., Hoffmann, P., Singer, W., and Bremer, J.: Long-term variations of the mesospheric wind
608 field at mid-latitudes, Ann. Geophys., 25, 1779–1790, 10.5194/angeo-25-1779-2007, 2007.
609 Kogure, M., Nakamura, T., Ejiri, M. K., Nishiyama, T., Tomikawa, Y., and Tsutsumi, M.: Effects of
610 horizontal wind structure on a gravity wave event in the middle atmosphere over Syowa (69°S,
611 40°E), the Antarctic. Geophysical Research Letters, 45, 5151–5157.
612 https://doi.org/10.1029/2018GL078264, 2018.
613 Koo, J.-H., Walker, K. A., Jones, A., Sheese, P. E., Boone, C. D., Bernath, P. F., and Manney, G.L.:
614 Global climatology based on the ACE-FTS version 3.5 dataset: Addition of mesospheric levels and
615 carbon-containing species in the UTLS, J. Quant. Spectrosc. Radiat. Transfer, 186, 52–62,
616 doi:10.1016/j.jqsrt.2016.07.003, 2017.
617 Kuttippurath, J. and Nikulin, G.: A comparative study of the major sudden stratospheric warmings in
618 the Arctic winters 2003/2004–2009/2010, Atmos. Chem. Phys., 12, 8115–8129,
619 https://doi.org/10.5194/acp-12-8115-2012, 2012.
620 Kvissel, O. K., Orsolini, Y. J., Stordal, F., Limpasuvan, V., Richter, J., and Marsh, D. R.: Mesospheric
621 intrusion and anomalous chemistry during and after a major stratospheric sudden warming. J.
622 Atmos. Solar-Terr. Phys., 78–79, 116–124, doi:10.1016/j.jastp.2011.08.015, 2012.
623 Lu, H., Bracegirdle, T.J., Phillips, T., and Turner, J.: A comparative study of wave forcing derived
624 from the ERA-40 and ERA-Interim reanalysis datasets. J. Climate, 28, 2291–2311,
625 https://doi.org/10.1175/JCLI-D-14-00356.1, 2015.

626 Limpasuvan, V., Orsolini, Y. J., Chandran, A., Garcia, R. R., and Smith, A. K.: On the composite
627 response of the MLT to major sudden stratospheric warming events with elevated stratopause, J.
628 Geophys. Res.-Atmos., 121, 4518–4537, doi:10.1002/2015JD024401, 2016.
629 Manney, G. L., Schwartz, M. J., Krüger, K., Santee, M. L., Pawson, S., Lee, J. N., Daffer, W. H.,
630 Fuller, R. A., and Livesey, N. J.: Aura Microwave Limb Sounder observations of dynamics and
631 transport during the record-breaking 2009 Arctic stratospheric major warming, Geophys. Res.
632 Lett., 36, L12815, doi:10.1029/2009GL038586, 2009.
633 Martineau, P., Son, S.-W., Taguchi, M., and Butler, A. H.: A comparison of the momentum budget in
634 reanalysis datasets during sudden stratospheric warming events, Atmos. Chem. Phys., 18, 7169–
635 7187, https://doi.org/10.5194/acp-18-7169-2018, 2018.
636 Matsuno, T.: A dynamical model of the stratospheric sudden warming, J. Atmos. Sci., 28, 1479–1494,
637 https://doi.org/10.1175/1520-0469(1971)028<1479:ADMOTS>2.0.CO;2, 1971.
638 Muscari, G., di Sarra, A., de Zafra, R. L., Lucci, F., Baordo, F., Angelini, F., and Fiocco, G.: Middle
639 atmospheric O_3, CO, N_2O, HNO_3, and temperature profiles during the warm Arctic winter 2001–
640 2002, J. Geophys. Res., 112, D14304, doi:10.1029/2006JD007849, 2007.
641 Newnham, D. A., Ford, G. P., Moffat-Griffin, T., and Pumphrey, H. C.: Simulation study for
642 measurement of horizontal wind profiles in the polar stratosphere and mesosphere using ground-
643 based observations of ozone and carbon monoxide lines in the 230–250 GHz region, Atmos. Meas.
644 Tech., 9, 3309–3323, doi:10.5194/amt-9-3309-2016, 2016.
645 Orsolini, Y. J., Limpasuvan, V., Pérot, K., Espy, P., Hibbins, R., Lossow, S., Larsson, K. R., and
646 Murtagh, D.: Modelling the descent of nitric oxide during the elevated stratopause event of January
647 2013, J. Atmos. Solar-Terr. Phys., 155, 50–61, doi:10.1016/j.jastp.2017.01.006, 2017.
648 Orsolini, Y. J., Urban, J., Murtagh, D. P., Lossow, S., and Limpasuvan, V.: Descent from the polar
649 mesosphere and anomalously high stratopause observed in 8 years of water vapor and temperature
650 satellite observations by the Odin Sub-Millimeter Radiometer, J. Geophys. Res., 115, D12305,
651 doi:10.1029/2009JD013501, 2010.
652 Pedatella, N. M., Chau, J. L., Schmidt, H., Goncharenko, L. P., Stolle, C., Hocke, K., Harvey, V. L.,
653 Funke, B., and Siddiqui, T. A.: How sudden stratospheric warming affects the whole atmosphere,
654 Eos, 99, available at https://doi.org/10.1029/2018EO092441, 2018.
655 Piddyachiy, V., Shulga, V., Myshenko, V., Korolev, A., Antyufeyev, O., Shulga, D., and Forkman, P.:
656 Microwave radiometer for spectral observations of mesospheric carbon monoxide at 115 GHz over
657 Kharkiv, Ukraine, J. Infrared Milli. Terahz. Waves, 38, 292–302, doi:10.1007/s10762-016-0334-1,
658 2017.
659 Piddyachiy, V. I., Shulga, V. M., Myshenko, V. V., Korolev, A. M., Myshenko, A. V., Antyufeyev, A.
660 V., Poladich, A. V., and Shkodin, V. I.: 3-mm wave spectroradiometer for studies of atmospheric

trace gases. Radiophys Quantum El., 53(5-6), 326–333. https://doi.org/10.1007/s11141-010-9231-y, 2010.

Rao, J., Ren, R., Chen, H., Yu, Yu., and Zhou, Y.: The stratospheric sudden warming event in February 2018 and its prediction by a climate system model, J. Geophys. Res.-Atmos., doi:10.1029/2018JD028908, 2018.

Ryan, N. J., Palm, M., Raffalski, U., Larsson, R., Manney, G., Millán, L., and Notholt, J.: Strato-mesospheric carbon monoxide profiles above Kiruna, Sweden (67.8°N, 20.4°E), since 2008, Earth Syst. Sci. Data, 9, 77–89, doi:10.5194/essd-9-77-2017, 2017.

Rinsland, C. P., Salawitch, R. J., Gunson, M. R., Solomon, S., Zander, R., Mahieu, E., Goldman, A., Newchurch, M. J., Irion, F. W., and Chang, A. Y.: Polar stratospheric descent of NO_y and CO and Arctic denitrification during winter 1992–1993, J. Geophys. Res., 104, 1847–1861, 1999.

Rüfenacht, R., Baumgarten, G., Hildebrand, J., Schranz, F., Matthias, V., Stober, G., Lübken, F.-J., and Kämpfer, N.: Intercomparison of middle-atmospheric wind in observations and models, Atmos. Meas. Tech., 11, 1971–1987, https://doi.org/10.5194/amt-11-1971-2018, 2018.

Rüfenacht, R., Kämpfer, N., and Murk, A.: First middle-atmospheric zonal wind profile measurements with a new ground-based microwave Doppler-spectroradiometer, Atmos. Meas. Tech., 5, 2647–2659, doi:10.5194/amt-5-2647-2012, 2012.

Salmi, S. M., Verronen, P. T., Thölix, L., Kyrölä, E., Backman, L., Karpechko, A. Yu., and Seppälä, A.: Mesosphere-to-stratosphere descent of odd nitrogen in February–March 2009 after sudden stratospheric warming, Atmos. Chem. Phys., 11, 4645–4655, https://doi.org/10.5194/acp-11-4645-2011, 2011.

Scheiben, D., Straub, C., Hocke, K., Forkman, P., and Kämpfer, N.: Observations of middle atmospheric H_2O and O_3 during the 2010 major sudden stratospheric warming by a network of microwave radiometers, Atmos. Chem. Phys., 12, 7753–7765, https://doi.org/10.5194/acp-12-7753-2012, 2012.

Shepherd, M. G., Beagley, S. R., and Fomichev, V. I.: Stratospheric warming influence on the mesosphere/lower thermosphere as seen by the extended CMAM, Ann. Geophys., 32, 589–608, doi:10.5194/angeo-32-589-2014, 2014.

Solomon, S., Garcia, R. R., Olivero, J. J., Bevilacqua, R. M., Schwartz, P. R., Clancy, R. T., and Muhleman, D. O.: Photochemistry and transport of carbon monoxide in the middle atmosphere, J. Atmos. Sci., 42, 1072–1083, 1985.

Stray, N. H., Orsolini, Y. J., Espy, P. J., Limpasuvan, V., and Hibbins, R. E.: Observations of planetary waves in the mesosphere-lower thermosphere during stratospheric warming events, Atmos. Chem. Phys., 15, 4997–5005, https://doi.org/10.5194/acp-15-4997-2015, 2015.

Tao, M., Konopka, P., Ploeger, F., Grooß, J.-U., Müller, R., Volk, C. M., Walker, K. A., and Riese, M.: Impact of the 2009 major sudden stratospheric warming on the composition of the stratosphere, Atmos. Chem. Phys., 15, 8695–8715, https://doi.org/10.5194/acp-15-8695-2015, 2015.

Tomikawa, Y., Sato, K., Watanabe, S., Kawatani, Y., Miyazaki, K., and Takahashi, M.: Growth of planetary waves and the formation of an elevated stratopause after a major stratospheric sudden warming in a T213L256 GCM, J. Geophys. Res., 117, D16101, doi:10.1029/2011JD017243, 2012.

Waters, J. W., Wilson, W. J., and Shimabukuro, F. I.: Microwave measurement of mesospheric carbon monoxide, Science, 191, 1174–1175, doi:10.1126/science.191.4232.1174, 1976.

WMO Commission for Atmospheric Sciences. Abridged Final Report of the Seventh Session, Manila, 27 February – 10 March, 1978. WMO-No. 509, 113 p., available at: http://library.wmo.int/pmb_ged/wmo_509_en.pdf, 1978.

Xu, X., Manson A. H., Meek C. E., Chshyolkova T., Drummond J. R., Hall C. M., Riggin D. M., and Hibbins R. E.: Vertical and interhemispheric links in the stratosphere-mesosphere as revealed by the day-to-day variability of Aura-MLS temperature data, Ann. Geophys., 27, 3387–3409, doi:10.5194/angeo-27-3387-2009, 2009.

Yu, Y., Cai, M., Shi, C., and Ren, R.: On the linkage among strong stratospheric mass circulation, stratospheric sudden warming, and cold weather events, Mon. Weather Rev., 146, 2717–2739, doi:10.1175/MWR-D-18-0110.1, 2018.

Yuan, T., Thurairajah, B., She, C. Y., Chandran, A., Collins, R. L., and Krueger, D. A.: Wind and temperature response of midlatitude mesopause region to the 2009 Sudden Stratospheric Warming, J. Geophys. Res., 117, D09114, doi:10.1029/2011JD017142, 2012.

Zhou, S., Miller, A. J., Wang, J., and James, K. A.: Downward-propagating temperature anomalies in the preconditioned polar stratosphere, J. Climate, 15, 781–792, doi:10.1175/1520-0442(2002)015<0781:DPTAIT>2.0.CO;2, 2002.

Zülicke, C. and Becker, E.: The structure of the mesosphere during sudden stratospheric warmings in a global circulation model, J. Geophys. Res.-Atmos., 118, 2255–2271, doi:10.1002/jgrd.50219, 2013.

Zülicke, C., Becker, E., Matthias, V., Peters, D. H. W., Schmidt, H., Liu, H.-L., de la Torre Ramos, L., and Mitchell, D. M.: Coupling of stratospheric warmings with mesospheric coolings in observations and simulations, J. Climate, 31, 1107–1133, doi:10.1175/JCLI-D-17-0047, 1, 2018.

Atmos. Chem. Phys. Discuss., https://doi.org/10.5194/acp-2018-1361
Manuscript under review for journal Atmos. Chem. Phys.
Discussion started: 7 February 2019

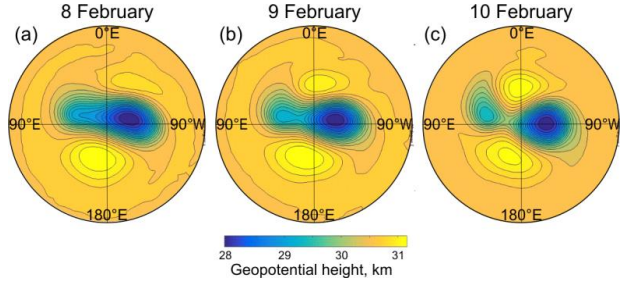

Figure 1. The polar vortex split at the 10-hPa pressure level during the SSW event in February 2018. Geopotential heights are calculated from ERA-Interim reanalysis data.

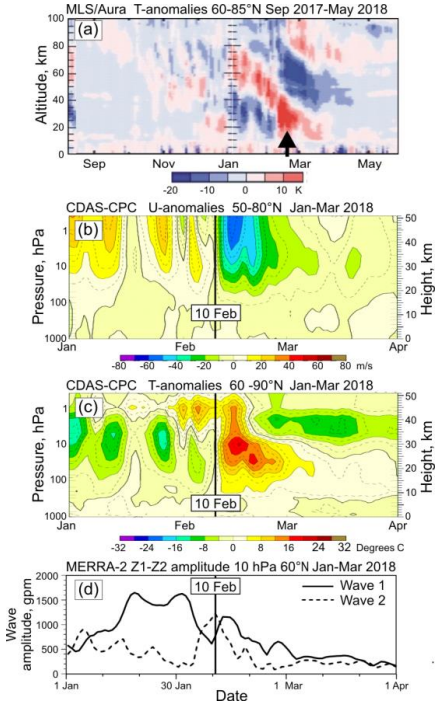

Figure 2. The development of the SSW in 2018 from the Northern polar stratosphere characteristics: (a) Aura MLS temperature anomalies in late August 2017–May 2018 at polar cap 60–85°N (climatology 2005–2017), (b) zonal mean zonal wind anomalies and (c) zonal mean temperature anomalies in January–March by NOAA NWS CPC data at

741 http://www.cpc.ncep.noaa.gov/products/stratosphere/strat-trop/ (climatology 1981–2010) and (d) zonal
742 wave-1 and wave-2 amplitudes in geopotential height at 10 hPa, 60°N, by the NASA GSFC ACP
743 statistics at https://acd-ext.gsfc.nasa.gov/Data_services/met/ann_data.html.
744

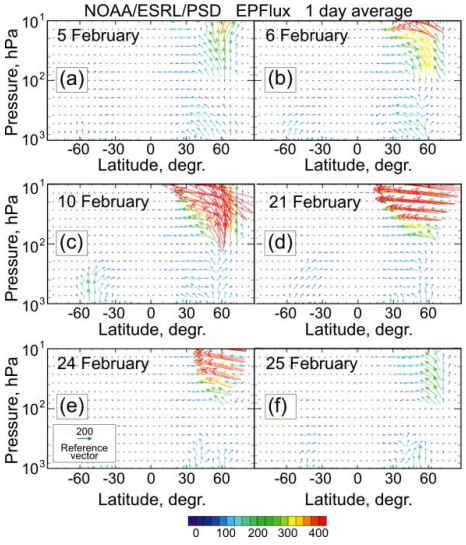

745
746
747 **Figure 3.** The changing NH wave activity in February 2018 by EP-flux data. From the NCEP–NCAR
748 reanalysis at https://www.esrl.noaa.gov/psd/data/epflux/.
749

Atmos. Chem. Phys. Discuss., https://doi.org/10.5194/acp-2018-1361
Manuscript under review for journal Atmos. Chem. Phys.
Discussion started: 7 February 2019

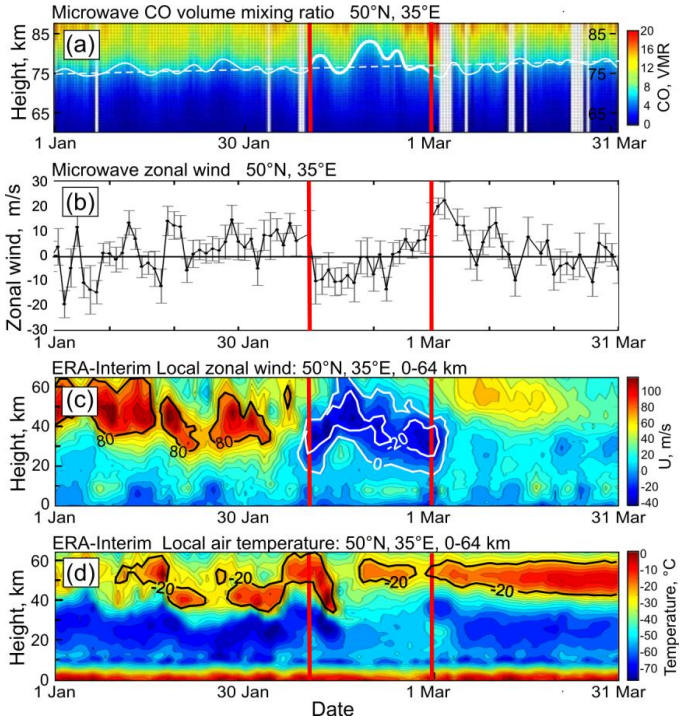

Figure 4. Mesospheric (a) CO profiles and (b) zonal wind microwave measurements over Kharkiv (averaged in altitude range 70–85 km, vertical bars are standard deviations) compared to (c) time-altitude local zonal wind, and (d) time-altitude local air temperature changes. Plots (c) and (d) are from the ERA-Interim reanalysis data averaged over longitudes 33.75–38.25°E and latitudes 48.00–52.25°N centered at the Kharkiv microwave radiometer site (35°E, 50°N). Time interval of significant variations in the atmosphere parameters due to the SSW event (from 10 February to 1 March, 2018) is bounded by red vertical lines.

Atmos. Chem. Phys. Discuss., https://doi.org/10.5194/acp-2018-1361
Manuscript under review for journal Atmos. Chem. Phys.
Discussion started: 7 February 2019

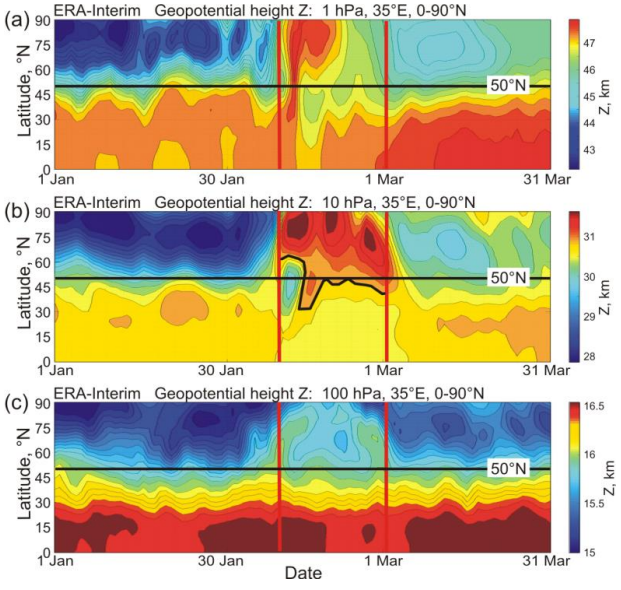

Figure 5. (a, b and c) Time–latitude variations in the NH geopotential heights Z at 1 hPa, 10 hPa, and 100 hPa, respectively, averaged in the 30–40°E longitudinal segment centered at the Kharkiv site longitude (35°E). From ERA-Interim reanalysis. The site latitude 50°N is marked by black solid line.

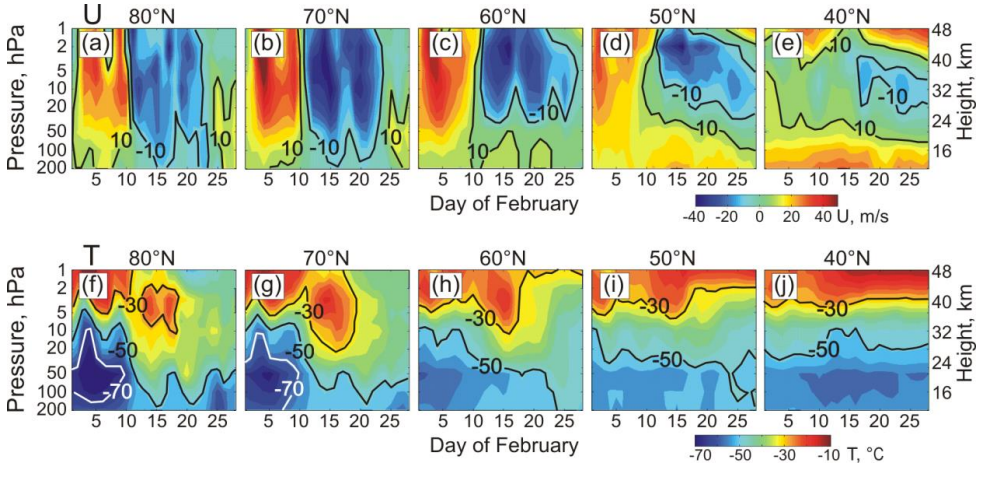

Figure 6. Variations of the zonally averaged vertical distribution of the stratospheric (a–e) zonal wind U and (f–j) air temperature T between the stratopause and tropopause (1–200 hPa pressure levels) in

Atmos. Chem. Phys. Discuss., https://doi.org/10.5194/acp-2018-1361
Manuscript under review for journal Atmos. Chem. Phys.
Discussion started: 7 February 2019

February 2018. The NH latitudes 80°, 70°, 60°, 50°, and 40° are presented. From ERA-Interim reanalysis.

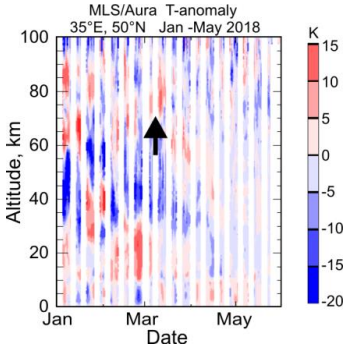

Figure 7. Air temperature anomalies over midlatitude station Kharkiv (35°E, 50°N) in January–May 2018 from the Aura MLS data (https://mls.jpl.nasa.gov/data/readers.php). Climatology 2005–2017 was used.